PNAS RESEARCH ARTICLE | APPLIED PHYSICAL SCIENCES MEDICAL SCIENCES

Sulfated oligosaccharide activates endothelial Notch for inducing macrophage-associated arteriogenesis to treat ischemic diseases

Yuanman Yu[a,b], Shuang Wang[c], Xinye Chen[b], Zehua Gao[c], Kai Dai[a], Jing Wang[a,b,1], and Changsheng Liu[b,c,1]

Edited by David Weitz, Harvard University, Cambridge, MA; received May 4, 2023; accepted October 1, 2023

Ischemic diseases lead to considerable morbidity and mortality, yet conventional clinical treatment strategies for therapeutic angiogenesis fall short of being impactful. Despite the potential of biomaterials to deliver pro-angiogenic molecules at the infarct site to induce angiogenesis, their efficacy has been impeded by aberrant vascular activation and off-target circulation. Here, we present a semisynthetic low-molecular sulfated chitosan oligosaccharide (SCOS) that efficiently induces therapeutic arteriogenesis with a spontaneous generation of collateral circulation and blood reperfusion in rodent models of hind limb ischemia and myocardial infarction. SCOS elicits anti-inflammatory macrophages' (Mφs') differentiation into perivascular Mφs, which in turn directs artery formation via a cell-to-cell communication rather than secretory factor regulation. SCOS-mediated arteriogenesis requires a canonical Notch signaling pathway in Mφs via the glycosylation of protein O-glucosyltransferases 2, which results in promoting arterial differentiation and tissue repair in ischemia. Thus, this highly bioactive oligosaccharide can be harnessed to direct efficiently therapeutic arteriogenesis and perfusion for the treatment of ischemic diseases.

ischemic diseases | in situ regeneration | therapeutic arteriogenesis | sulfated oligosaccharide | perivascular macrophage

Significance

Rapid establishment of collateral arterial circulation is crucial for the treatment of ischemic diseases. However, conventional pro-angiogenic drugs mostly suffer from abnormal angiogenesis and potential cancer risk, and currently, no off-the-shelf biomaterials can efficiently induce angiogenesis. In this study, we show that sulfated oligosaccharides can regulate the polarization of host Mφs and differentiate into perivascular cells, thereby effectively inducing in situ arterial regeneration. Sulfated oligosaccharides activate Notch signaling to facilitate arterial regeneration and development through communication between perivascular Mφs and arterial endothelial cells. We expect that these findings may pave the way for the development of biomaterial-based therapeutic arteriogenesis to treat ischemic diseases.

Ischemic vascular diseases, such as coronary artery disease, cerebral ischemia, and peripheral arterial disease, have long been one of the most severe diseases with high morbidities and mortalities (1). Therapeutic strategies for inducing arteriogenesis and collateral reconstruction, restoration of the blood supply, and alleviation of the ischemic injury are of crucial importance in ischemic disease interventions (2–5). There has long been an interest in developing effective treatment of systemic delivery with exogenous pro-angiogenic molecules [e.g., vascular endothelial growth factor (VEGF) and fibroblast growth factor] to rapidly reconstruct the functional vasculature network (6, 7). However, this growth factor-based therapeutics is still far from satisfactory. Notably, high doses of angiogenic agents are commonly used for efficiently inducing therapeutic angiogenesis owing to their short half-life and rapid elimination at the ischemic site, which inescapably disrupts the homeostasis balance of local microenvironment with an increased risk of oedema and tumor formation (8). Moreover, the existing therapeutic strategies mainly focus on inducing highly branched capillary beds (9, 10), and there is still a lack of therapeutic modalities for directing the formation of functional arteries to meet the demands of sufficient circulation in the ischemic diseases.

The ischemic diseases are invariably associated with the infiltration of inflammatory cells, among which macrophages (Mφs) exhibit a pivotal role in immunomodulation and directly contribute to arteriogenesis through secretion of a multitude of pro-angiogenic cytokines (11–13). Additionally, Mφs can also modulate arteriogenesis and tissue repair through intercellular communication (14). Expanding the scope of immunotherapies to encompass ischemic injuries by promoting the therapeutic functions in Mφs, thereby enhancing functional blood perfusion, would undoubtedly be an attractive prospect for a range of acute ischemic diseases. However, the insufficient regulation of Mφs with spontaneous secretion of angiogenic factors results in inadequate neovascularization and hinders complete recovery from ischemia. Additionally, uncontrolled release of inflammatory cytokines can lead to excessive tissue fibrosis and even atherosclerosis, ultimately impeding successful tissue repair. Nowadays, materiobiology-based therapeutic strategy has proven to be auspicious objectives for in situ ischemic treatment, utilizing the physicochemical properties of biomaterials to accurately regulate the recruiting Mφs that produce a series of metalloproteinases, vasoactive substances, chemokines, and growth factors to rebuild the collateral circulation (15). However, the process of arteriogenesis involves multicellular assembly to form a complex structure with three concentric layers

Author contributions: Y.Y., J.W., and C.L. designed research; Y.Y., S.W., X.C., Z.G., and K.D. performed research; Y.Y. analyzed data; and Y.Y., J.W., and C.L. wrote the paper.

The authors declare no competing interest.

This article is a PNAS Direct Submission.

[1]To whom correspondence may be addressed. Email: biomatwj@163.com or liucs@ecust.edu.cn.

This article contains supporting information online at https://www.pnas.org/lookup/suppl/doi:10.1073/pnas.2307480120/-/DCSupplemental.

Published November 9, 2023.

(i.e., endothelial cells, smooth muscle cells, and connective tissues) (16), which imposes higher demands on biomaterials for regulating the host microenvironment and inducing mature arteries. Furthermore, the role of biomaterial-regulated Mφs in arteriogenesis remains unknown, particularly for implanted biomaterials. Therefore, it is imperative to design proper biomaterials in a way to regulate Mφ behaviors to promote arteriogenesis and reveal its potential regulatory mechanisms.

Natural polysaccharides with specific structural features ubiquitously exist in mammalian tissues, in which sulfated polysaccharides often serve as a reservoir to anchor endogenous growth factors with the unique abilities to regulate the bioactivity of endogenous cytokines to efficiently induce angiogenesis (17, 18). Previous studies also have indicated that sulfated polysaccharides possess Mφ-regulatory activities by binding and activating specific carbohydrate receptors on the surface of Mφs (19), giving rise to a reduction in pro-inflammatory cytokine secretion and an increase in the release of pro-angiogenic factors, ultimately promoting vascularization (20, 21). Actually, polysaccharides are susceptible to enzymatic or hydrolytic degradation in vivo (22), resulting in the formation of oligosaccharides that further participate in wound healing. As a degradation product, oligosaccharides can efficiently regulate the pathological microenvironment and therapeutically alleviate inflammatory responses (23), oxidative stress (24), and hypertension (25) in the treatment of ischemic diseases. Apart from that, oligosaccharides also play pivotal roles in maintaining the arterial wall integrity and regulating cellular behavior within it (26, 27). However, the mechanisms by which oligosaccharides interact with host cells and modulate endogenous growth factors to induce in situ arteriogenesis remain largely elusive.

In a previous study, we investigated the efficacy of various chitosan-derived polysaccharides in inducing therapeutic angiogenesis in ischemia, which suggested that the presence of a sulfated group and saccharide sequence is essential for promoting angiogenesis (21). We hypothesize that the properties of oligosaccharides can also independently influence arteriogenesis by regulating the pathological microenvironment, which we examined two oligosaccharides [chitosan oligosaccharides (COS) and sulfated COS (SCOS)] with distinct electrical charges. Here, we aimed to investigate the role of SCOS in promoting arteriogenesis and enhancing blood perfusion recovery in ischemic tissues. Additionally, we sought to elucidate the mechanism by which SCOS regulates the in vivo microenvironment and stimulates the formation of blood vessels. Our findings suggest that SCOS regulates perivascular Mφs to induce arteriogenesis via a canonical Notch signaling pathway. Therefore, by designing bioactive oligosaccharides, we can create an implant that efficiently induces the artery formation and in turn addresses the ischemic diseases.

Results

SCOS Promotes Arteriogenesis Following Ischemia Injury in Mice. The synthesized SCOS was subjected to various analytical techniques, including gel permeation chromatography, elemental analysis, ξ-potential analysis, NMR, and Fourier transform infrared spectroscopy (FT-IR). A representative NMR and FT-IR graph revealed that the SCOS was successfully modified with sulfated groups (*SI Appendix*, Fig. S1). Zeta potential measurements revealed that SCOS and COS exhibited a negative charge and a positive charge, respectively, which also indicated that the cationic hydroxyl group on COS was replaced by an anionic sulfated group.

To assess the pro-angiogenic activity of SCOS and COS, we first implanted the scaffolds into the ischemic hind limbs (Fig. 1*A*). Blood perfusion degrees in the ischemic hind limb normalized to the contralateral limb were examined by Laser Speckle imaging with quantitative analysis on days 1, 3, 7, and 14 postoperations (Fig. 1*B*). The results showed that the impaired hind limb perfusion caused a 50% and 40% postoperative reduction at the ischemic sites and the paw, respectively. In mice implanted with SCOS GS, perfusion measured at the implanted site and paw progressively increased over time, and reach its peak on day 7 after implantation (Fig. 1 *C* and *D*). In contrast, an attenuated recovery of perfusion was observed in both Blank GS and COS GS, which meant that collateral circulation was not efficiently reconstructed.

To better understand how SCOS GS restored the perfusion, we examined the vasculature of implants retrieved on days 7 and 14. Synchrotron radiation–based microcomputed tomography showed a clear invasion of microvessels from the host artery into the implants (Fig. 1*E*). The quantitative analysis reveled significantly higher relative blood vessel volume and vascular number in SCOS GS compared to COS GS and Blank GS. Moreover, these parameters exhibited a gradual increase from day 7 to day 14 postimplantation (Fig. 1 *F* and *G*). Next, we also assessed the levels of α-SMA- and CD31-positive arteries in the implants retrieved from the ischemic hind limb after implantation for 7 d and 14 d, respectively. We found that abundant CD31-positive endothelial cells spontaneously organized into vascular networks that were stabilized with α-SMA-positive cells to form typical arteries in SCOS GS on day 7 compared to Blank GS and COS GS (Fig. 1 *H* and *I*). The number of arteries involved in COS GS had no significant difference compared to the Blank GS. Flow cytometry analysis also confirmed a higher quantity of $CD31^{hi}Sca\text{-}1^{hi}$ arteriole cells in SCOS GS on day 7 after implantation in the ischemic hind limb, with a slight decrease observed on day 14 (*SI Appendix*, Fig. S2). Simultaneously, the dissolved free oxygen in the SCOS-treated ischemic muscle tissue was observed to steadily increase over time until it reaches the normal physiological level and maintains equilibrium, as demonstrated by a gold-standard oxygen microelectrode (Fig. 1*J*). Considering the observed decline in arteriole density after 14 d, it is plausible to assert that capillaries also play a crucial role in maintaining oxygen levels within the surrounding tissues during the later stages.

Histological examination of hematoxylin and eosin (H&E) staining was conducted to analyze the invasion of new blood vessels and tissues into the implants. The newly formed blood vessels are predominantly located within the fibrous connective tissue that has developed between the implant and muscle space (Fig. 1*K*). As expected, a higher density of ingrowth microvessels and fibrous tissue was found in SCOS GS compared to Blank GS and COS GS, and an obvious collateral with a thick arterial wall and mature erythrocytes could be observed in SCOS GS on day 7 after surgery (Fig. 1*K*). Together, these findings suggest that SCOS significantly promotes the formation of arteries and rescues the perfusion in severe ischemia.

SCOS Modulates the Mφs Polarization and Inflammatory Response. Once biomaterials were implanted, the myeloid cells gathered and participated in the regulation of tissue repair (28). To examine whether myeloid cells were involved in the process of SCOS-mediated arteriogenesis in ischemia, implants were retrieved on day 7 postoperation and the recruited cells were analyzed for innate immune cell markers using a flow cytometry analysis. Dendritic cells ($CD11b^{+}CD11c^{+}$), neutrophils ($CD11b^{+}Ly6G^{+}$), and Mφs ($CD11b^{+}F4/80^{+}$) in each group had no significant differences, which meant that the oligosaccharide had no effect on the recruitment of myeloid cells (Fig. 2 *A* and *C* and *SI Appendix*, Fig. S3). As Mφs could subsequently polarize to diverse phenotypes and exhibit different functions in angiogenesis, we further analyzed the phenotype of infiltrating Mφs

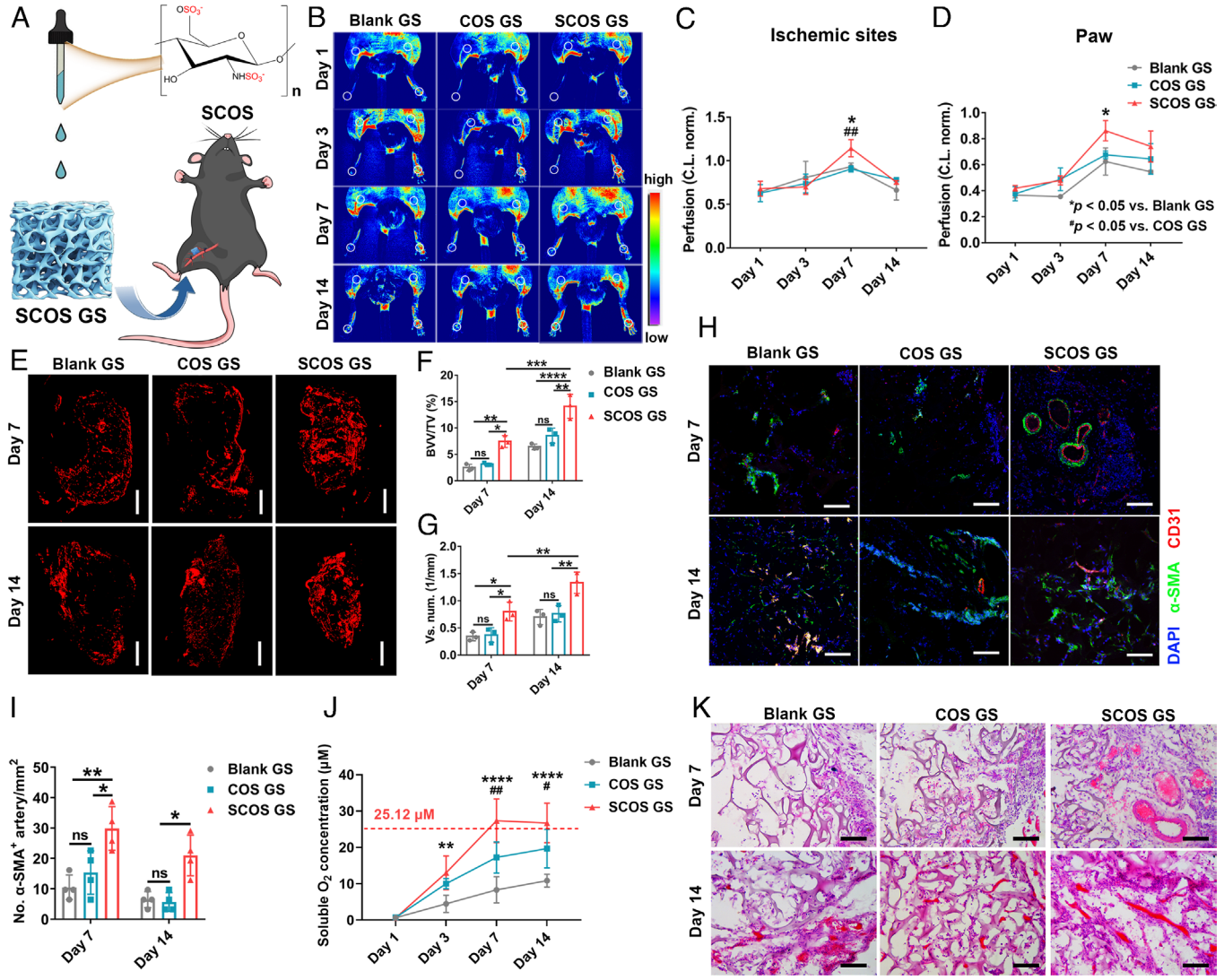

Fig. 1. SCOS promotes arteriogenesis and blood reperfusion in hind limb ischemia. (*A*) Illustration of the preparation of SCOS GS and implantation into the mice hind limb ischemia model. (*B*) Laser Speckle imaging of ischemic implanted sites and paw over time. (*C* and *D*) Quantification of perfusion levels of the ischemic sites (*C*) and paw (*D*) (n = 4). *$P < 0.05$ vs. Blank GS; #$P < 0.05$ vs. COS GS. C.L. norm., contralateral (non-ischemic) limb normalized. (*E–G*) Representative angiographic images (*E*) and quantitative analysis (*F* and *G*) of relative blood vessel volume (BVV/TV) and vascular number (Vs. num.) in implants on day 7 and day 14 (n = 4). (Scale bars, 1 mm.) (*H* and *I*) Representative immunostainings (*H*) and quantitative analysis (*I*) of α-SMA$^+$ arteries in implants (n = 5). (Scale bars, 100 μm.) (*J*) Quantification of the dissolved oxygen levels at the ischemic sites over time, with a detection depth of 3 mm. The dotted red line and red number represent the quantification of intramuscular dissolved oxygen in the hind limb of the sham group. (*K*) Hematoxylin and eosin (H&E) staining of implants on days 7 and 14 after implantation in the ischemic hind limb. (Scale bars, 100 μm.) Blank GS, PBS immersed gelatin sponge; COS GS, COS-coated gelatin sponge; SCOS GS, SCOS-coated gelatin sponge. Data represent mean ± SD. *$P < 0.05$, **$P < 0.01$, ***$P < 0.005$, and ****$P < 0.001$; ns, not significant [(*C* and *D*), one-way ANOVA with Tukey's post hoc test; (*F*, *G*, and *J*), two-way ANOVA with Tukey's post hoc test].

in implants in ischemia. Flow cytometry analysis revealed that both SCOS GS and COS GS significantly attenuated the M1 Mφ (CD197$^+$CD206$^-$) polarization, while SCOS GS triggered a higher extent of M2 Mφ (CD197$^-$CD206$^+$) polarization relative to the other groups (Fig. 2 *B*, *D*, and *E*). Immunostainings of the retrieved implants on day 7 also confirmed that more dominant CD206-positive M2 Mφs could be observed in the SCOS GS than in the other groups, contrary to the CD197-positive M1 polarization pattern (Fig. 2*F*). Additionally, gene-profiling of Mφs isolated from SCOS GS showed higher expression of M2-type genes, including *Tie2*, *Arg1*, *Hgf*, *Pdgfb*, *Vegfa*, *Mmp2*, and *Sdf*, than Blank GS and COS GS (Fig. 2*G*). Conversely, several pro-inflammatory or anti-angiogenic (that is, M1-type) molecules were down-regulated in SCOS GS-treated Mφs; these included *Il1b*, *Tnfa*, *Cxcl10*, and *Ifnb* (Fig. 2*G*).

To further clarify the mechanism how SCOS regulated the behavior of Mφs polarization, we also examined the oligosaccharide-dependent Mφ polarization in vitro. To determine the optimal dosage of oligosaccharide, mouse peritoneal Mφs (mpMφs) were co-cultured with a series concentration of SCOS or COS for 1 d, 3 d, and 7 d. We found that mpMφs co-cultured with SCOS at the concentration of 800 ng/mL significantly enhanced the cell viability of Mφs in vitro on day 3 and day 7; in contrast, COS appeared to have no effect on cell viability of Mφs (*SI Appendix*, Fig. S4*A*). Moreover, the live/dead assay also revealed a substantial population of viable cells (indicated by green dots) in the cohort treated with SCOS at a concentration of 800 ng/mL for a duration of 3 d (*SI Appendix*, Fig. S4*B*). Thus, the concentration of 800 ng/mL oligosaccharides was screened for the subsequent in vitro experiments. The stimulation of Mφ polarization in vitro was subsequently confirmed by a flow cytometry analysis; the results indicated that both SCOS and COS decreased the in vitro M1 polarization of Mφs, while only SCOS had a discernible effect on M2 polarization of Mφs (*SI Appendix*, Fig. S5 *A–C*). It is noteworthy that the overall expression of M1 macrophages was higher

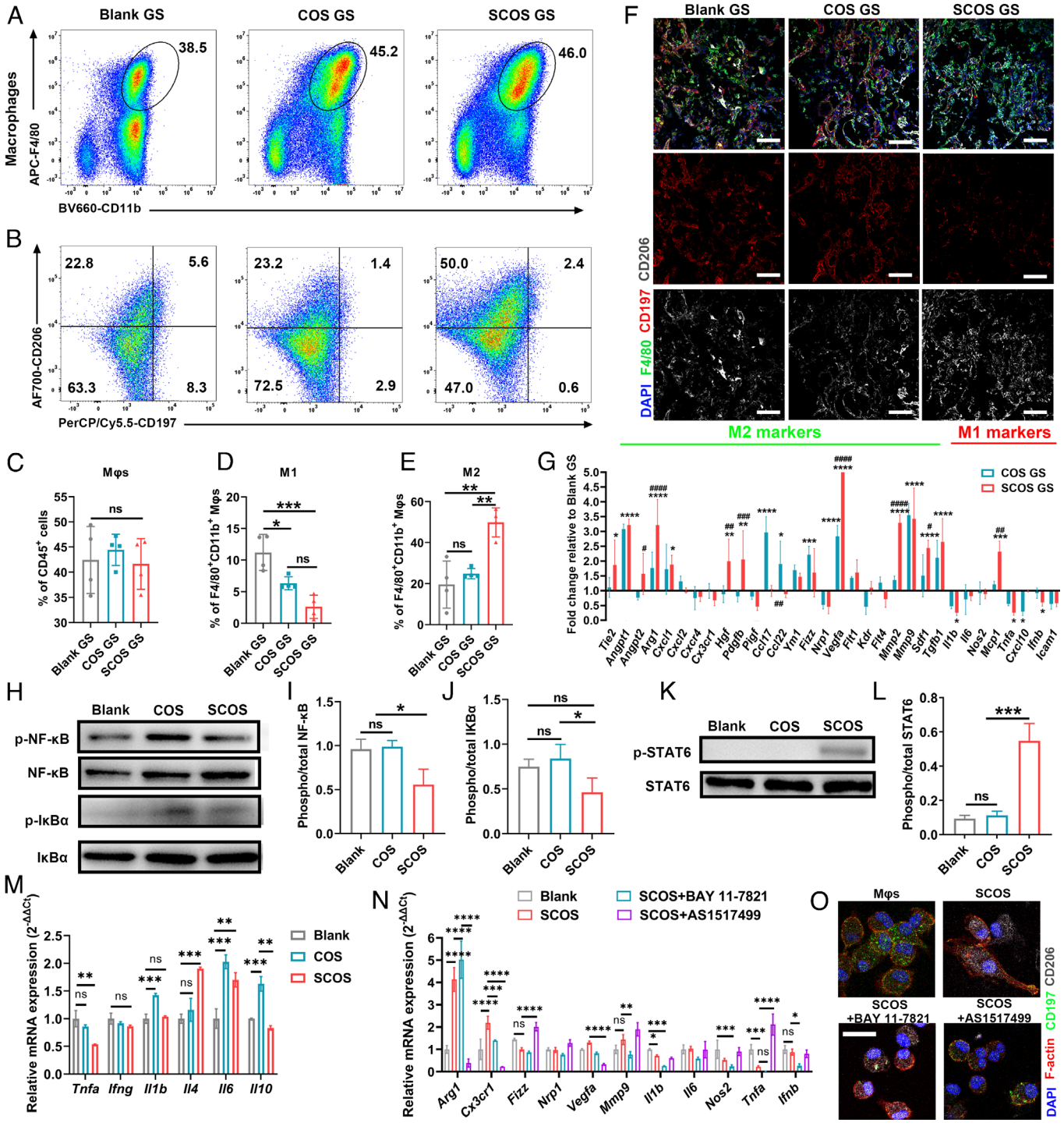

Fig. 2. SCOS increased the recruitment of anti-inflammatory Mφs to the implants. (*A*) Representative flow cytometry plots of $CD11b^+F4/80^+$ cells (Mφs) from implants on day 7 after implantation in ischemic limb (n = 4). (*B*) Representative flow cytometry plots of $CD197^+CD206^-$ Mφs (M1) and $CD197^-CD206^+$ Mφs (M2) polarization in implants (n = 4). (*C–E*) Quantification of $CD11b^+F4/80^+$ Mφs (*C*) and M1/M2 polarization (*D* and *E*) in implants on day 7 after implantation in ischemia. (*F*) Representative immunostainings of F4/80, CD197, and CD206 in implants on day 7. (Scale bars, 200 μm.) (*G*) Gene profile by quantitative PCR of $F4/80^+$ macrophages sorted from oligosaccharide-coated GS on day 7 after the implantation into the hind limb ischemia. (*H–L*) Representative western blots analysis and the relative level of phosphorylated NF-κB signaling pathway (*I* and *J*) and phosphorylated STAT6 (*L*) after treating with the indicated oligosaccharides for 1 h. (*M*) Relative gene expression of Mφs stimulated with COS or SCOS in vitro for 3 d. (*N*) Relative inflammatory-related gene expression in Mφs after the treatment of SCOS with NF-κB (BAY 11-7821) and STAT6 (AS1517499) inhibitors for 3 d. (*O*) Representative immunostaining of Mφs polarization treated with NF-κB (BAY 11-7821) and STAT6 (AS1517499) inhibitors for 3 d. (Scale bars, 20 μm.) $^*P < 0.05$ vs. Blank GS; $^{\#}P < 0.05$ vs. COS GS. Data represent mean ± SD. $^*P < 0.05$, $^{**}P < 0.01$, $^{***}P < 0.005$, $^{****}P < 0.001$; ns, not significant (one-way ANOVA with Tukey's post hoc test).

in vitro than in vivo, primarily attributable to the preferential induction of M1-type by abdominal macrophages stimulated with nutrient broth. Additionally, immunostainings showed more CD206 puncta on the Mφs after the treatment of SCOS for 3 d (*SI Appendix*, Fig. S5*D*), indicating attenuation of M1 polarization by SCOS.

Canonical nuclear factor kappa-light-chain-enhancer of activated B (NF-κB) and signal transducers and activators of transcription 6 (STAT6) signaling pathways are known to function in inflammatory and healing activation (29–31), we therefore examined the mechanism of how SCOS regulated Mφ polarization. The results of

western blot analysis revealed that SCOS statically inhibited the NF-κB activation and increased the expression of p-STAT6 (Fig. 2 *H–L*). We next investigated the inflammation-related gene expression of Mφs with the treatment of oligosaccharide for 3 d, including canonical pro-inflammatory genes (*Tnfa*, *Ifny*, *Il1b*, and *Il6*) and anti-inflammatory genes (*Il4* and *Il10*). Quantitative real-time polymerase chain reaction (qPCR) analysis showed that SCOS significantly decreased the pro-inflammatory gene expression of Tnfa, while COS up-regulated partial pro-inflammatory genes (*Il1b* and *Il6*) (Fig. 2*M*). In contrast, the expression of the gene associated with anti-inflammatory cytokines (*Il4*) in Mφs was significantly elevated after the treatment of SCOS for 3 d (Fig. 2*M*). To further validate the engagement of NF-κB and STAT6 signaling pathways in SCOS-mediated regulation of Mφ polarization, we employed small-molecular inhibitors BAY 11-7821 and AS1517499 to suppress the expression of NF-κB and STAT6 signaling, respectively. Interestingly, both qPCR analysis and immunostainings revealed that the beneficial effect of SCOS on M2 Mφ polarization was nullified by the treatment with the inhibitor targeting STAT6 signaling (Fig. 2 *N* and *O*). Additionally, the inhibition of NF-κB signaling using BAY 11-7821 resulted in a more pronounced enhancement of SCOS-mediated regulation of M2 Mφ polarization (Fig. 2 *N* and *O*). Thus, the results indicate that SCOS induces the transition of M1-to-M2 Mφ polarization via a downregulation of NF-κB signaling with the phosphorylation of STAT6 signaling.

Conditioned Medium (CM) from SCOS-Treated Mφs Altered the Arteriogenic Behavior In Vitro. To investigate how Mφs affected arteriogenesis, a model of ex vivo aortic ring angiogenesis assay was conducted with the treatment of Mφs and oligosaccharides. We found that SCOS co-cultured with Mφs significantly promoted the formation of microvessels sprouted from the arterial rings (*SI Appendix,* Fig. S6). Strikingly, obvious tip cells could be observed in the SCOS-treated group, which meant that SCOS and Mφs are beneficial to the formation of new arterioles. Next, to explore the factors in Mφs that influenced the arteriogenic behavior of endothelial cells, we collected the CM pretreated with SCOS or COS to culture mouse arterial endothelial cells (MAECs). With the treatment of SCOS/Mφs CM, the number of sprouts, number of branch points, and total network length in the sprouting fibrin bead assay showed a significant higher level than that with the treatment of other groups (*SI Appendix,* Fig. S7). Thus, SCOS-stimulated Mφs were conducive to arterial sprouting. Esm1 is a tip cell marker and VEGF-regulated gene product, which efficiently mediates the sprouting during angiogenesis (32). Notably, upregulation of *Esm1* and *Vegf* was also detectable in SCOS/Mφs CM-treated MAECs (*SI Appendix,* Fig. S8).

Tubular network formation and migration of endothelial cells are also the key steps of the arteriogenesis process. Strikingly, all Mφs CM exhibited an inhibited ability to induce the formation of network and migration of endothelial cells compared to the Blank (*SI Appendix,* Fig. S9). Among them, SCOS/Mφs CM slightly alleviated the inhibition effect on the cell migration (*SI Appendix,* Fig. S9 *D* and *E*). In addition, all CM collected from Mφs with or without the stimulation of oligosaccharides statistically restrained the cell viability of MACEs (*SI Appendix,* Fig. S9*F*). We also observed that the oligosaccharides themselves did not cause significant cytotoxicity on MAECs at a series concentration (*SI Appendix,* Fig. S10), which meant the cytokines secreted from Mφs may hinder the arterial function of MAECs.

Next, to further verify the role of Mφs involved in SCOS-induced arteriogenesis, we continuously administered clodronate liposomes every 2 d to totally deplete the circulating Mφs and evaluated the simultaneous angiogenesis (*SI Appendix,* Fig. S11*A*). Laser Speckle imaging analysis revealed that depletion of circulating Mφs was detrimental to reconstruct collateral circulation and restore blood perfusion (*SI Appendix,* Fig. S11 *B–D*). In addition, implants containing Mφ-secreted CM from oligosaccharide stimulation slightly increased the blood perfusion but have no statistical difference relative to that in implants without adding the Mφ-secreted CM (*SI Appendix,* Fig. S11 *B–D*). Immunostainings of α-SMA and CD31 also showed a significant impairment in arteriogenesis in all Mφ-depletion mice (*SI Appendix,* Fig. S11 *E–G*). The addition of COS/Mφ CM or SCOS/Mφ CM did not rescue the luminal and wall growth in collaterals (*SI Appendix,* Fig. S11*E*). Thus, these results reveal that cytokines secreted by Mφs negligibly affect SCOS-induced arteriogenesis in ischemia, which prompt us to hypothesize that Mφs might affect arteriogenesis in another manner.

Mφs Act as Perivascular Cells to Support Arteriogenesis. In addition to cytokines secretion, evidence that has emerged in recent years point to the fact that Mφs can also serve as perivascular cells to support vessel anastomosis and maturation (33, 34). To further the relevance of oligosaccharide-stimulated Mφs for arteriogenesis in ischemia, we selectively and transiently depleted circulating Mφs with clodronate liposomes injection and designed cell transfer experiments (Fig. 3*A*). We only give intraperitoneal injection of PBS at the initial stage (d0-d3 after implantation) to ensure that the Mφs can efficiently secrete cytokines to stimulate the cell sprouts from existing blood vessels and recruit endothelial cells to the injured sites. Subsequently, clodronate liposomes were continuously injected (d4-d6 after implantation) to totally deplete the circulating Mφs to exclude the influence of Mφ–endothelial cell interactions on directing arterial formation and maturation. Afterward, Mφs pretreated with COS or SCOS in vitro were injected into ischemic limb muscles (d7 after implantation) to examine the regulatory role of Mφs with different treatment in regulating arteriogenesis. Hind limb perfusion measurements by laser Speckle imaging revealed a progressive increase at the implanted site and paw on the first 7 d (Fig. 3 *B–D*). However, the blood perfusion in all groups showed a visible impairment after the depletion of circulating Mφs, which was improved by transfer of SCOS pretreated Mφs on day 9 (Fig. 3 *B–D*). In contrast, transfer of Mφs or COS pretreated Mφs had a negligible effect on the promotion of limb perfusion. Immunostainings revealed that α-SMA$^+$ cell-encapsulated arteries were difficult to observe in the PBS-injected group with a significant decrease of CD31$^+$ endothelial cells ingrowth into the implants after the depletion of host circulating Mφs, which provided evidence that Mφs are indispensable for arteriogenesis (Fig. 3 *E–G*). Transfer of Mφs or COS pretreated Mφs also rescued arteriogenesis, although to a lesser extent (Fig. 3 *E–G*). Interestingly, an adoptive transfer of SCOS pretreated Mφs efficiently rescued arteriogenesis, enabling the formation of mature arteries with a larger inner circumference (Fig. 3*E*). Notably, we observed that a subset of α-SMA$^+$ cells did not participate in arterial assembly following the adoptive transfer of SCOS pretreated Mφs (Fig. 3*E*), indicating that this approach of adoptive Mφs transfer does not fully rescue the process of Mφ-associated arteriogenesis.

To better capture a possible interaction between Mφs and blood vessels, we investigated the characteristic distribution and densities of perivascular Mφs. Immunostainings revealed that the numbers of F4/80$^+$ Mφs infiltration into the SCOS-treated Mφs group exhibited a higher level relative to the other groups after the injection of adoptive Mφs, which indicated that the SCOS-treated Mφs had a more excellent cell viability and migration capacity compared to the other groups (Fig. 3 *H* and *I*). Consistently, an abundant density of F4/80$^+$ perivascular Mφs was observed to be located adjacent to

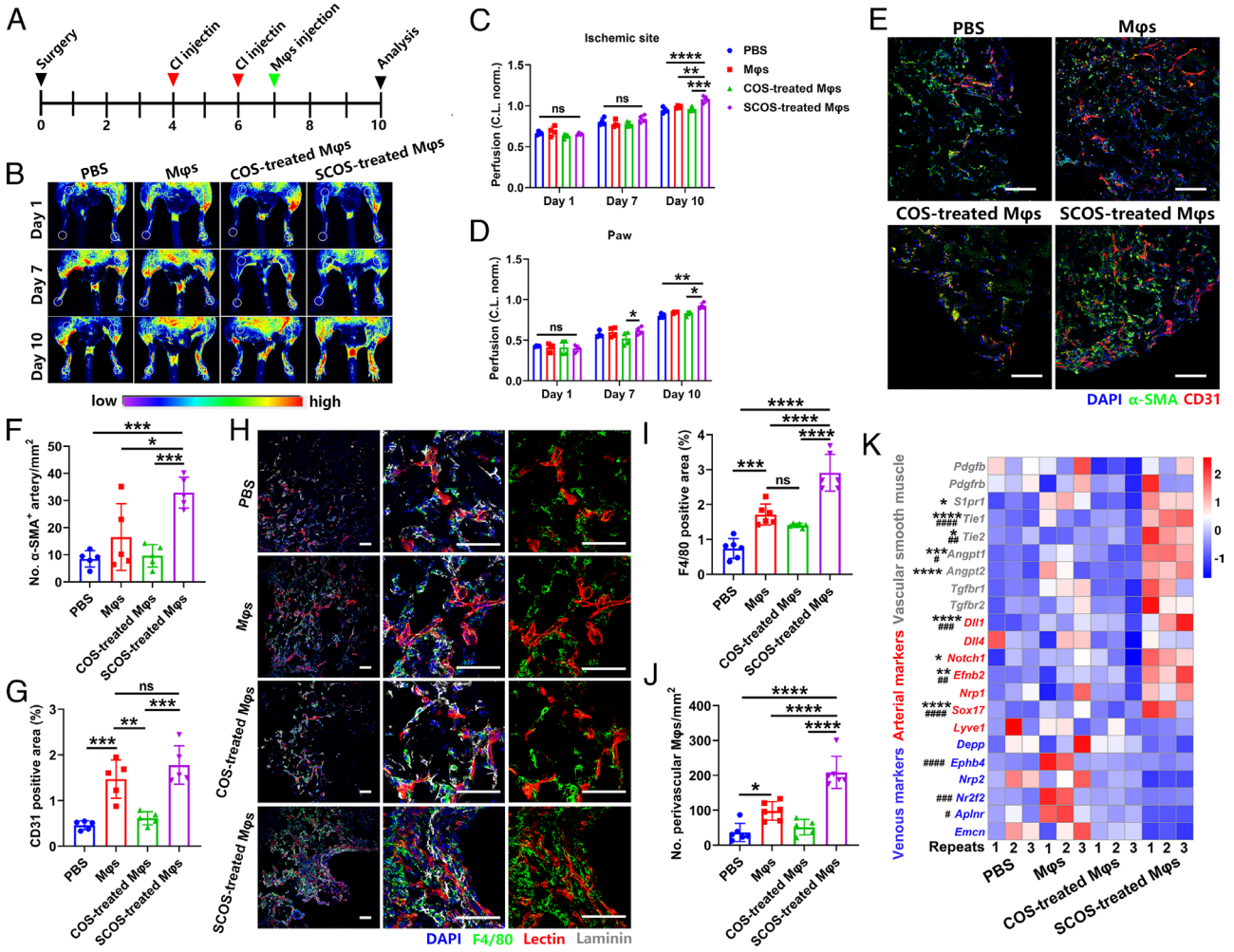

Fig. 3. SCOS-stimulated perivascular Mφs play a vital role in regulating arteriogenesis. (*A*) Schematic with host circulating Mφs depletion and adoptive oligosaccharide-stimulated Mφs transfer strategies. Cl: clodronate liposomes. (*B*) Laser Speckle imaging of ischemic implanted sites and paw over time. (*C* and *D*) Quantification of perfusion levels of the ischemic sites (*C*) and paw (*D*) (n = 4). (*E*) Representative fluorescent images of implants stained with α-SMA (green), CD31 (red), and DAPI (blue) with the rescue of host circulating Mφs depletion by transfer of adoptive oligosaccharide-stimulated Mφs. (Scale bars, 100 μm.) (*F* and *G*) Quantitative analysis of α-SMA$^+$ arteries (*F*) and relative CD31-positive area (*G*) in implants (n = 5). (*H*) Representative fluorescent images of implants stained with F4/80 (green), lectin (red), laminin (white), and DAPI (blue). (Scale bars, 50 μm.) (*I* and *J*) Quantification analysis of the relative F4/80-positive area (*I*) and F4/80$^+$ perivascular Mφs (*J*) on day 7 after implantation (n = 5). (*K*) qPCR analysis of arterial and venous markers in implants retrieved from Mφ-rescued mice. Data represent mean ± SD. *P < 0.05, **P < 0.01, ***P < 0.005, ****P < 0.001; ns, not significant (*C* and *D*, unpaired two-tailed Student's t test; *F*, *G*, *I*–*K*, one-way ANOVA with Tukey's post hoc test).

lectin$^+$ blood vessels with the treatment of SCOS and embedded within the laminin$^+$ vascular basement membranes relative to that in Mφs and COS-treated Mφs (Fig. 3 *H* and *J*). We further analyzed the polarization phenotype of perivascular Mφs and measured the density of M1 or M2 Mφs by their expression of CD197 or CD206. The results showed that the perivascular Mφs in SCOS-treated Mφs were virtually positive for CD206 (*SI Appendix*, Fig. S12). Additionally, expression of genes involved in pericyte differentiation (*Tie1*, *Tie2*, *Angpt1*, and *Angpt2*) or arterial endothelial markers [*Dll1* (Delta-like 1), *Notch1*, *Efnb2*, and *Sox17*] was increased in SCOS-treated Mφs, whereas expression of genes involved in venous endothelial markers (*Ephb4*, *Nr2f2*, and *Aplnr*) was decreased in SCOS-treated Mφs (Fig. 3*K*). Together, these results suggest that Mφs play a predominant role as perivascular cells in SCOS-induced arteriogenesis.

SCOS Regulates Perivascular Mφ-Mediated Arteriogenesis Via a Canonical Notch Pathway. As Notch signaling is a cell-to-cell contact-dependent signaling pathway and positively regulates arterial formation (35, 36), we thus explored the relevance between endothelial Notch signaling and perivascular Mφs in the context of arteriogenesis with the induction of oligosaccharide. Immunostainings confirmed that most active Notch1 proteins were strongly localized in lectin$^+$ vessels adjacent to perivascular Mφs, and not all intramural microvessels were positive for Notch1 protein expression (Fig. 4 *A*–*C*). Notably, the active Notch1 expression on endothelial cells was itself subject to SCOS regulation. The density of Notch1 protein on the surface of lectin$^+$ vessels significantly increased with the treatment of SCOS GS, whereas COS GS seemed to have a negligible effect on activating Notch1 expression (Fig. 4 *A* and *D*). Comparative gene expression profiling in ischemia with the implantation of SCOS GS revealed high expression of Notch1 and its ligand *Dll1* relative to COS GS and Blank GS, while the levels of transcripts for the Notch ligands Dll4 were comparable (Fig. 4*E*).

To further confirm whether Mφs were necessary for activating endothelial Notch signaling, we analyzed the Notch-related gene expression in the direct co-cultured Mφs and MAECs with or without oligosaccharides treatment. mRNA analysis of Notch1, as well as several downstream mediators of Notch signaling (*Hes1*, *Hes5*, *Hey1*, and *Hey2*), was up-regulated in MAECs with the co-culture of SCOS and Mφs (Fig. 4*F*). Inversely, the stimulation

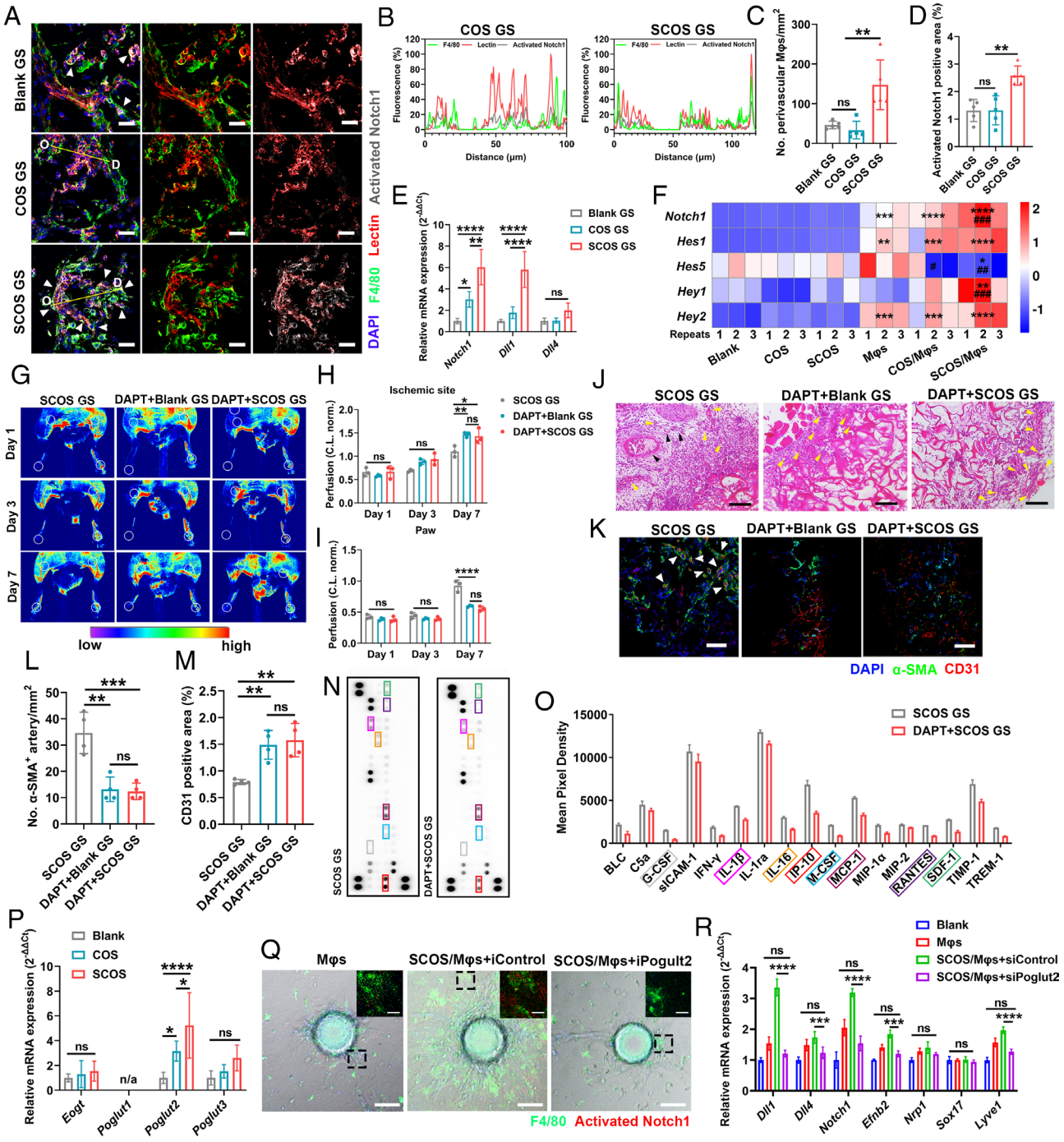

Fig. 4. Role of SCOS regulating Mφs in a *Notch*-controlled arteriogenesis. (*A–D*) Representative immunostainings (*A*) with quantification of F4/80$^+$ perivascular Mφs (*C*) and activated Notch1 expression (*D*) on day 7 after implantation (n = 5). The fluorescence intensities of protein expression along the line segments (*O-D*) in the images were presented (*B*). (Scale bars, 20 μm.) (*E*) qPCR analysis for the expression of *Notch1*, *Dll1*, and *Dll4* transcripts extracted from GS after the implantation for 7 d in ischemia. (*F*) The *Notch*-related gene expression of MAECs after co-culturing with oligosaccharides and Mφs for 3 d. *$P < 0.05$ vs. Blank; $^{\#}P < 0.05$ vs. Mφs. (*G*) Laser Speckle imaging of ischemic implanted sites and paw over time. (*H* and *I*) Quantification of perfusion levels of the ischemic sites (*H*) and paw (*I*) (n = 3). (*J*) H&E staining of SCOS GS on days 7 after implantation in the ischemic hind limb with or without treatment of *N*-[*N*-(3,5-Difluorophenacetyl-L-alanyl)]-(*S*)-phenylglycine *t*-butyl ester (DAPT). (Scale bars, 100 μm.) (*K*) Representative fluorescent images of SCOS GS stained with α-SMA (green), CD31 (red), and DAPI (blue) after treating with or without DAPT. (Scale bars, 100 μm.) (*L* and *M*) Quantitative analysis of α-SMA$^+$ arteries (*L*) and relative CD31-positive area (*M*) in implants (n = 4). (*N* and *O*) Mouse cytokine array analysis of retrieved samples from SCOS GS and SCOS GS treated with DAPT after the implantation for 7 d in ischemia (*N*). Selected cytokines marked with colored outlines. Quantification of cytokine levels was carried out by densitometry (*O*). (*P*) Expression of *Notch*-related galactosyltransferase genes in Mφs with treatment of COS or SCOS for 3 d. (*Q*) Representative immunostainings of F4/80$^+$ mpMφs and activated Notch1 expression in a sprouting fibrin bead model for 7 d. MpMφs and MAECs were co-cultured and pretransfected with *Poglut2* siRNA for 24 h. Insets are outlined by dashed black lines shown at higher magnification. (Scale bars, 100 μm.) [Scale bars (zoomed snapshot), 20 μm.] (*R*) Arterial-related gene expression of MAECs. MpMφs were pretransfected with *Poglut2* siRNA and stimulated simultaneously with SCOS for 24 h. MAECs were co-cultured with *Poglut2*-silenced mpMφs for another 24 h and detected the arterial gene expression in isolated MAECs. Data represent mean ± SD. *$P < 0.05$, **$P < 0.01$, ***$P < 0.005$, ****$P < 0.001$, ns, not significant (unpaired two-tailed Student's *t* test).

of SCOS or COS alone did not induce a significant difference in related genes expression of MAECs. Moreover, flow cytometry analysis revealed that SCOS and COS were more likely to bind to Mφs compared to MAECs (*SI Appendix*, Fig. S13), which meant that the oligosaccharides preferentially stimulated the Mφs rather than arterial endothelial cells.

To further address the role of Notch signaling in Mφ-mediated arteriogenesis, we pharmacologically inhibited the expression of Notch by administration of the γ-secretase inhibitor DAPT. As the results mentioned above showed no significant effect of COS GS on Mφ-mediated arteriogenesis, we focus on SCOS GS as a potential regulator of Notch signaling for further study. Laser Speckle imaging analysis revealed that the blood perfusion at the implanted site progressively increased over time with the treatment of DAPT (Fig. 4 *G* and *H*). In contrast, exposing implants to the DAPT caused a statistically inhibition in blood flow reconstruction at the paw (Fig. 4 *G* and *I*). A previous study has established that inhibition of Notch signaling directs tip-derived endothelial cells into developing veins, while activation of Notch signaling couples sprouting angiogenesis and artery formation (35). The increase of blood perfusion in the ischemic site was attributed to the large number of capillaries' ingrowth induced by DAPT, while the loss of Notch disrupted the reconstruction of collateral circulation and thus led to impaired blood flow recovery in the hind limb. Strikingly, we found that SCOS GS had no significant improvement in restoring blood perfusion compared to Blank GS after the treatment of DAPT (Fig. 4 *G–I*). Similarly, histomorphometric analysis of arteriogenesis after the treatment of DAPT showed a significant impairment in luminal and wall growth in collaterals (Fig. 4*J*). Immunostainings analysis also revealed that inhibition of Notch signaling weakened the capacity of SCOS GS in inducing α-SMA$^+$ cells surrounded arteries, and SCOS GS exhibited no significant difference in inducing angiogenesis and artery formation compared to Blank GS with the treatment of DAPT (Fig. 4 *K–M*). Together, these results suggest that inhibition of Notch signaling restricts the promotion of SCOS in inducing arteriogenesis.

As SCOS could efficiently promote the polarization of M1-to-M2 Mφs with an obvious down-regulation of inflammatory response, we next investigated the essential role of inflammatory regulation in SCOS-induced arteriogenesis. Cytokine analysis of supernatant from harvested SCOS GS confirmed a widespread down-regulation of numerous inflammatory cytokines (most notably IL-1β, IL-16, IP-10, RANTES, and SDF-1) with the treatment of DAPT (Fig. 4 *N* and *O*). In addition, we found that the level of monocyte chemoattractant protein-1 and macrophage colony–stimulating factor in the DAPT-treated group was decreased relative to that in SCOS GS, which is the main chemokines for recruitment and differentiation of Mφs. These results again confirm the importance of Mφs in arteriogenesis, and the secreted cytokines is not the most important factor in this process.

Notch is a cell-surface receptor that assembled by O-glycans attached to epidermal growth factor-like (EGF) repeats in its extracellular domain (37, 38), in which protein O-fucosyltransferase (POFUT) plays an important role in regulating the binding of the Notch ligand. To gain further insight into the mechanism how SCOS affected arteriogenesis via a canonical Notch signaling, we examined the gene expression of Notch-related O-glycosylation. In the endoplasmic reticulum, the EGF repeats in the Notch receptor extracellular domain are properly modified with O-N-acetylglucosamine (GlcNAc) by EOGT (epidermal growth factor-domain specific O-GlcNAc transferase) and O-glucose by POGLUT (protein O-glucosyltransferase) (39). QPCR analysis revealed that SCOS treatment substantially up-regulated the expression of *Poglut2* and hardly affected the *Eogt* (Fig. 4*P*), indicating that SCOS active O-glucose-related glycosylation in Mφs. To examine the effect of *Poglut2* on SCOS-related glycosylation, we utilized a co-culture system of mpMφ/MAEC to validate the influence of *Poglut2* on SCOS-mediated activation of Notch signaling. In comparison with the Notch signaling triggered by exogenous DLL1 on the surface of mpMφs and MAECs, SCOS-induced Notch signaling predominantly manifested on the surface of F4/80$^+$ mpMφs (*SI Appendix,* Fig. S14). As anticipated, silencing the expression of the *Poglut2* gene effectively hindered the SCOS-induced activation of Notch1 in mpMφs (Fig. 4*Q* and *SI Appendix,* Fig. S14). Additionally, we found that disruption of glycosylation by *Poglut2* siRNA in mpMφs also markedly inhibited the expression of arterial endothelial markers in MAECs and exhibited a similar level compared to the groups of Mφs and Blank in mpMφs/MAECs co-culture system (Fig. 4*R*), which indicated that the inhibition of the glycosylation of Notch protein in Mφs restricted the SCOS-mediated arteriogenesis. Together, these results suggest that SCOS regulates perivascular Mφ-mediated arteriogenesis via a canonical Notch pathway.

SCOS Rescues Cardiac Function in a Model of Myocardial Infarction (MI). Given the potential utility of SCOS to rescue perfusion in the ischemic limb, we sought to investigate whether this oligosaccharide could improve outcomes in the more demanding setting of MI, a representative ischemic model that also involved in Mφ-associated pro-angiogenesis and wound healing (40, 41). To verify the effects of SCOS on the remodeling after MI, we generated a photo-cross-linked hyaluronic acid (HA) hydrogel mixed with SCOS and compared the repair capability to healthy mice (Sham) and MI mice that received HA hydrogel injection alone. At 28 d after the surgery, terminal histological analysis with Masson's trichrome staining revealed that treatment with SCOS HA significantly reduced the collagen density in the infarct area and sustained the thickness of the interventricular septum (Fig. 5*A*). Immunostainings of CD31-positive vessels in the ischemic zone of the cardiac tissue indicated a substantial increase in α-SMA$^+$ cell–encapsulated arteries ingrowth in SCOS-treated infarcted hearts compared to that in HA group (Fig. 5 *B* and *C*). Furthermore, echocardiographic analysis was administrated to determine cardiac functional parameters on day 14 and day 28 after MI (Fig. 5*D* and *SI Appendix*, Fig. S15). As a cardiac function indicator, left ventricular ejection fractions (LVEFs) in empty HA hydrogel–treated MI heart exhibited a half value of the sham group (Fig. 5*E*). In contrast, SCOS HA resulted in partial rescue of cardiac function, with LVEFs and left ventricular fractional shortening (LVFS) close to that measured in the sham controls (Fig. 5 *E* and *F*). Immunostainings revealed that treatment with the SCOS HA efficiently reduced myocardial apoptosis (Fig. 5*G*). With the treatment of SCOS HA, the reentry of cardiomyocytes into the cell cycle was unambiguously confirmed by analysis of PCM1-expressing cardiomyocytes that were positive for EdU and exhibited Aurora B at the midline between cardiomyocyte nuclei (Fig. 5*H* and *SI Appendix*, Fig. S16). These results suggest substantial rescue of cardiac function with SCOS treatment following a major ischemic injury in MI mice.

To further validate the role of Mφs in MI regulated by SCOS, we investigated the impact of SCOS on Mφ polarization in models of MI. Flow cytometry analysis revealed a significant increase in the proportion of Mφs in the MI model compared to the sham group, while no significant difference was observed between the SCOS HA group and the HA group (*SI Appendix*, Fig. S17 *A* and *C*). A swift of M1-to-M2 Mφ polarization with an obvious expression of activated Notch1 in CD206$^+$ Mφs was also observed in SCOS-treated infarcted hearts (*SI Appendix*, Figs. S17 *B*, *D*, and *E* and S18), which was consistent with the aforementioned findings in limb ischemia models. The collective findings suggest that the activation of Notch signaling by SCOS promotes Mφ-associated arteriogenesis as a potential therapeutic approach for MI.

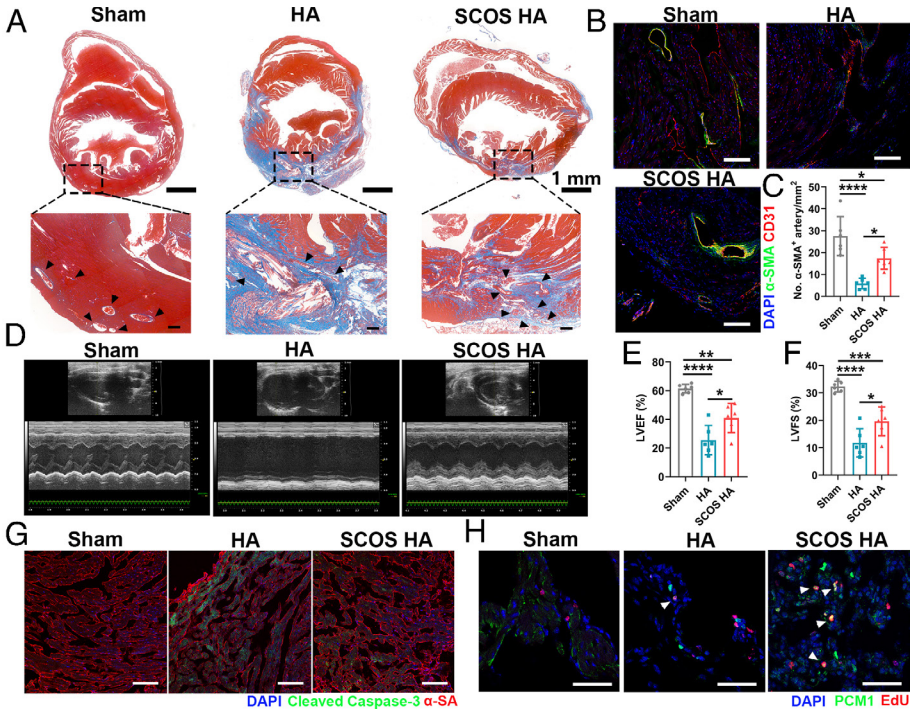

Fig. 5. SCOS HA rescues cardiac function after MI in mice on day 28. (*A*) Representative Masson's trichrome–stained myocardial sections on day 28 after MI or sham surgery. Snapshots, high-magnification images of the black box area. Black arrow: Blood vessels. (Scale bar, 100 μm.) (*B* and *C*) Representative immunostainings (*B*) and quantitative analysis (*C*) of α-SMA$^+$ arteries in the myocardial scar and border zone on day 28 after MI or sham surgery (n = 6). (Scale bars, 100 μm.) (*D*) Typical M-mode echocardiography of the hearts was obtained from mice on day 28 after MI or sham surgery. (*E* and *F*) LVEF (*E*) and LVFS (*F*) were measured using echocardiography on day 28 after MI or sham surgery. (*G*) Representative immunostainings of cleaved caspase-3 (green) and α-SA (red) staining to visualize cardiomyocyte apoptosis on day 28. α-SA, sarcomeric α-actinin. (Scale bars, 100 μm.) (*H*) Representative immunostainings of EdU incorporation in the PCM1$^+$ cardiomyocyte (white arrow) on day 14. (Scale bars, 50 μm.) Data represent mean ± SD. *P < 0.05, **P < 0.01, ***P < 0.005, ****P < 0.001; ns, not significant (one-way ANOVA with Tukey's post hoc test).

Discussion

Implants that efficiently induce blood vessel growth into ischemic sites and rescue sufficient circulation is a prerequisite process for the treatment of ischemic disease (3, 4, 9, 42, 43). Mφs, as one of the first responders to injury, exhibit remarkable plasticity that enables them to efficiently respond to implant signals and facilitate collateral vessel remodeling (44, 45). Therefore, there is a pressing need to develop a potential biomaterial-based therapeutic strategy that can effectively activate Mφs and thus induce arteriogenesis. Here, our study demonstrates that SCOS can serve as a pro-angiogenic agent by regulating perivascular Mφs through canonical Notch signaling, promoting arteriogenesis in both mice models of lower limb ischemia and MI (*SI Appendix,* Fig. S19). During ischemic neovascularization, Mφs commonly regulate endothelial cells through two mechanisms: secreting cytokines to stimulate the sprouts of endothelial cells or acting as perivascular cells to support the maturation of blood vessels. Our findings suggest that the Notch signaling induced by SCOS between perivascular Mφs and arterial endothelial cells primarily controls the formation of mature and highly developed arteries within the ischemic cavity, rather than the cytokine-mediated endothelial cell behavior. Depletion of circulating Mφs significantly abrogated the formation of arteries and reconstruction of collateral circulation. Notably, an adoptive transfer of SCOS-treated Mφs restored vascularization in Mφ-depleted mice, while administration of SCOS-treated CM had no discernible effect on promoting the regeneration of arteries. This biomaterial, which promotes arteriogenesis without the use of extra growth factors, represents a promising therapeutic approach for ischemic diseases.

Accumulating evidence suggests that Mφs can be classified into two distinct subpopulations: a canonical pro-inflammatory phenotype (M1) and an alternative pro-healing phenotype (M2), and M2 Mφs can further be subdivided into M2a, M2c, and M2f (13). Although different subtypes of M2 Mφs play varying roles in directing arteriogenesis, it is believed that CD206-positive M2a Mφs are particularly relevant to arteriogenesis due to their perivascular positioning and ability to induce collateral circulation reconstruction during ischemia (46). Apart from that, Mφs and its polarized phenotype-related differential cytokines secretion in particular are responsible for collateral vessel remodeling during arteriogenesis (11, 47–49). In the present study, the indispensable role of Mφs in inducing SCOS-mediated arteriogenesis did not preclude participation of the cytokines secreted by Mφs in ischemic mice. Nevertheless, our findings demonstrated that supplementation of COS or SCOS-stimulated Mφs CM at a late stage had no appreciable effect on the collateral vessel reconstruction and blood flow recovery in the absence of Mφs. Additionally, we observed that mpMφ-stimulated CM exerted a negative regulatory effect on arterial cell-related behaviors in vitro. As previous studies have reported that excess secretion of inflammatory cytokines from Mφs will also promote lipoprotein retention, degrade the extracellular matrix, and eventually lead to atherosclerosis (50, 51), we speculated that the pro-inflammatory cytokines secreted from Mφs may also have restricted the process of arteriogenesis. Although SCOS/Mφs CM efficiently alleviated the Mφ-related inhibition of inflammation by regulating Mφ polarization to M2 via the STAT6 signaling pathway, its remarkable promotion of arteriogenesis in vivo was not consistently observed. Our data collectively indicate that the cytokines released

from Mφs, particularly during the later stages, are unlikely to be primarily responsible for the SCOS-related arteriogenesis in ischemia.

In addition to secreted molecular pathways, the behavior of endothelial cells is also controlled by cell-to-cell communication parameters, which has roles in angiogenesis and numerous vascular pathologies. Emerging evidence indicates that a distinct population of perivascular Mφs residing proximal to blood vasculature is crucial for improving blood flow regulation and functional recovery of ischemic tissues (34, 46, 52). The perivascular Mφs have been established to promote vessel stabilization, which in turn functions as a barrier for potential harmful blood-born substances in the tissues. However, their involvement in biomaterial-mediated arteriogenesis has not yet been described. Here, we have demonstrated that SCOS provoked the accumulation of CD206-positive expressed perivascular Mφs along with arterioles during collateral vessel remodeling in ischemia. A previous study has reported that perivascular Mφs critically induced venous-to-arterial differentiation with the presence of arterial vascular smooth muscle cells in the parenchyma (52). Unlike the SCOS/Mφs CM induction, adoptive transfer of SCOS-stimulated Mφs significantly restores the blood perfusion and vasculature reconstruction in Mφ-depleted mice, which confirmed that this cell-to-cell communication played a vital role in inducing arteriogenesis.

The process of arteriogenesis is always associated with the biomechanical-mediated signaling pathway. Once an injury occurs, instructive cues expressed by local resident immune cells orchestrate the injury response of endothelial cells or other resident progenitor cells during tissue regeneration, which is partly mediated by endothelial-specific expression of Notch or integrin signaling. Previous studies have shown that the endothelial Notch signaling pathway fosters Mφ maturation during ischemia, which in turn promotes arteriogenesis (14). This study showed that activated Notch highly expressed between perivascular Mφs and arterial endothelial cells in SCOS GS, which was able to coordinate arteriogenesis and tissue regeneration in ischemia. Notch is a cell-surface receptor that is regulated by O-glycans attached to EGF repeats in its extracellular domain (37). The binding of Notch ligands is regulated by POFUT, POGLUT, or EOGT (38, 53, 54). Notably, SCOS significantly improved the expression of *Poglut2*, and our experiments with *Poglut2* siRNA-treated Mφs abrogated the glycosylation of Notch receptors and statistically reduced the arterial-related gene expression in MAECs. Using a Notch inhibitor DAPT resulted in a dysfunctional vasculature and hindered the promotion of SCOS in arteriogenesis. Therefore, we conclude that SCOS is directly involved in the O-glucose or O-GlcNAc modifications within EGF repeats via the glycosylation of POGLUT2, leading to increased ligand-induced Notch signaling and enhanced therapeutic arteriogenesis in ischemia.

In summary, we here described a semisynthesized sulfated oligosaccharide that efficiently induced arteriogenesis and rapidly achieved blood flow penetration in ischemia. We also revealed an approach for biomaterial regulating perivascular Mφ-mediated arteriogenesis, which is different from conventional cytokine-mediated angiogenesis. Although information on the definite mechanism of how SCOS involved in the synthetic process of EGF repeats and thus regulates Notch activity was not experimentally demonstrated in this study, it was clear that SCOS could recruit the local resident Mφs to transform into perivascular Mφs and induce arteriogenesis by activating the expression of Notch signaling within the Mφ-to-endothelial cell communications. We believe that these findings provide insight into the Mφ-mediated arteriogenesis induced by immunomodulation of SCOS and may be adopted as a potential therapeutic target for ischemic defects and diseases.

Materials and Methods

Detailed materials and methods are provided in *SI Appendix, Materials and Methods*, including the *Materials*; *Mouse Hind Limb Ischemia*; *Micro-CT Analysis*; *Mouse MI Model*; *Echocardiography*; *Histology and Immunofluorescence Analysis*; *Flow Cytometry Analysis*; *Cell Isolation and Culture*; *Mφs Polarization*; *Western Blot Analysis*; *Rat Aortic Ring Angiogenesis Assay*; *Conditioned Media Collection from Mφs*; *Sprouting Fibrin Bead Assay*; *Tube Formation Assay*; *Scratch Wound Assay*; *Mφs Depletion*; *Adoptive Transfer Experiments*; Poglut2 *Gene Silence Experiment*; *Quantitative RT-PCR Analysis*; *Cell Binding Assay*; and *Statistical Analysis*. All surgical procedures were approved by the Institutional Animal Care and Use Committee of East China University of Science and Technology.

Data, Materials, and Software Availability. All study data are included in the article and/or *SI Appendix*.

ACKNOWLEDGMENTS. This research was supported by the Basic Science Center Program of National Natural Science Foundation of China (No. T2288102), the Key Program of the National Natural Science Foundation of China (No. 32230059), the National Natural Science Foundation of China (No. 32101086), the National Postdoctoral Program for Innovative Talents (BX2021101), and the China Postdoctoral Science Foundation Funded Project (2021M701192), Fundamental Research Funds for the Central Universities (JKD01221507), and the Foundation of Frontiers Science Center for Materiobiology and Dynamic Chemistry (JKVD1211002). This study was also supported by the 111 Project (B14018).

Author affiliations: [a]The State Key Laboratory of Bioreactor Engineering, East China University of Science and Technology, Shanghai 200237, People's Republic of China; [b]Frontiers Science Center for Materiobiology and Dynamic Chemistry, East China University of Science and Technology, Shanghai 200237, People's Republic of China; and [c]Key Laboratory for Ultrafine Materials of Ministry of Education, East China University of Science and Technology, Shanghai 200237, People's Republic of China

1. C. W. Tsao *et al.*, Heart disease and stroke statistics–2022 update: A report from the American Heart Association. *Circulation* **145**, e153–e639 (2022).
2. M. Mahmoudi *et al.*, Multiscale technologies for treatment of ischemic cardiomyopathy. *Nat. Nanotechnol.* **12**, 845–855 (2017).
3. R. Zhang *et al.*, Particle-based artificial three-dimensional stem cell spheroids for revascularization of ischemic diseases. *Sci. Adv.* **6**, eaaz8011 (2020).
4. D. Zhu *et al.*, Nitrate-functionalized patch confers cardioprotection and improves heart repair after myocardial infarction via local nitric oxide delivery. *Nat. Commun.* **12**, 4501 (2021).
5. D. Zhi *et al.*, Mechanically reinforced biotubes for arterial replacement and arteriovenous grafting inspired by architectural engineering. *Sci. Adv.* **8**, eabl3888 (2022).
6. Y. D. Lin *et al.*, Instructive nanofiber scaffolds with VEGF create a microenvironment for arteriogenesis and cardiac repair. *Sci. Transl. Med.* **4**, 146ra109 (2012).
7. H. Jin *et al.*, Release of basic fibroblast growth factor from acoustically-responsive scaffolds promotes therapeutic angiogenesis in the hind limb ischemia model. *J. Control. Release* **338**, 773–783 (2021).
8. H. Karvinen *et al.*, Long-term VEGF-A expression promotes aberrant angiogenesis and fibrosis in skeletal muscle. *Gene Ther.* **18**, 1180 (2011).
9. J. B. Lee *et al.*, Microchannel network hydrogel induced ischemic blood perfusion connection. *Nat. Commun.* **11**, 615 (2020).
10. B. G. Soliman *et al.*, Development and characterization of gelatin-norbornene bioink to understand the interplay between physical architecture and micro-capillary formation in biofabricated vascularized constructs. *Adv. Healthc. Mater.* **11**, 2101873 (2022).
11. Y. Takeda *et al.*, Macrophage skewing by Phd2 haplodeficiency prevents ischaemia by inducing arteriogenesis. *Nature* **479**, 122–126 (2011).
12. M. Potente, H. Gerhardt, P. Carmeliet, Basic and therapeutic aspects of angiogenesis. *Cell* **146**, 873–887 (2011).
13. P. L. Graney *et al.*, Macrophages of diverse phenotypes drive vascularization of engineered tissues. *Sci. Adv.* **6**, eaay6391 (2020).
14. K. Krishnasamy *et al.*, Blood vessel control of macrophage maturation promotes arteriogenesis in ischemia. *Nat. Commun.* **8**, 952 (2017).
15. Y. Li, Y. Xiao, C. Liu, The horizon of materiobiology: A perspective on material-guided cell behaviors and tissue engineering. *Chem. Rev.* **117**, 4376–4421 (2017).
16. D. Wang *et al.*, Microfluidic bioprinting of tough hydrogel-based vascular conduits for functional blood vessels. *Sci. Adv.* **8**, eabq6900 (2022).

17. Y. Yu *et al.*, Manipulation of VEGF-induced angiogenesis by 2-N, 6-O-sulfated chitosan. *Acta Biomater.* **71**, 510–521 (2018).
18. D. Hachim, T. E. Whittaker, H. Kim, M. M. Stevens, Glycosaminoglycan-based biomaterials for growth factor and cytokine delivery: Making the right choices. *J. Control. Release* **313**, 131–147 (2019).
19. S. Zamze *et al.*, Recognition of bacterial capsular polysaccharides and lipopolysaccharides by the macrophage mannose receptor. *J. Biol. Chem.* **277**, 41613–41623 (2002).
20. Ø. Arlov, D. Rütsche, M. Asadi Korayem, E. Öztürk, M. Zenobi-Wong, Engineered sulfated polysaccharides for biomedical applications. *Adv. Funct. Mater.* **31**, 2010732 (2021).
21. Y. Yu *et al.*, Sulfated polysaccharide directs therapeutic angiogenesis via endogenous VEGF secretion of macrophages. *Sci. Adv.* **7**, eabd8217 (2021).
22. M. Naveed *et al.*, Chitosan oligosaccharide (COS): An overview. *Int. J. Biol. Macromol.* **129**, 827–843 (2019).
23. W. Han *et al.*, The anti-inflammatory activity of specific-sized hyaluronic acid oligosaccharides. *Carbohydr. Polym.* **276**, 118699 (2022).
24. L. Zhu *et al.*, Effect of Chitosan oligosaccharides on ischemic symptom and gut microbiota disbalance in mice with hindlimb ischemia. *Carbohydr. Polym.* **240**, 116271 (2020).
25. S. Guo *et al.*, Entering the spotlight: Chitosan oligosaccharides as novel activators of CaCCs/TMEM16A. *Pharmacol. Res.* **146**, 104323 (2019).
26. J. E. Wagenseil, R. P. Mecham, Vascular extracellular matrix and arterial mechanics. *Physiol. Rev.* **89**, 957–989 (2009).
27. J. M. Mattson, R. Turcotte, Y. Zhang, Glycosaminoglycans contribute to extracellular matrix fiber recruitment and arterial wall mechanics. *Biomech. Model. Mechanobiol.* **16**, 213–225 (2017).
28. E. Dondossola *et al.*, Examination of the foreign body response to biomaterials by nonlinear intravital microscopy. *Nat. Biomed. Eng.* **1**, 7 (2016).
29. C. Porta *et al.*, Tolerance and M2 (alternative) macrophage polarization are related processes orchestrated by p50 nuclear factor κB. *Proc. Natl. Acad. Sci. U.S.A.* **106**, 14978–14983 (2009).
30. Z. Czimmerer *et al.*, The transcription factor STAT6 mediates direct repression of inflammatory enhancers and limits activation of alternatively polarized macrophages. *Immunity* **48**, 75–90.e6 (2018).
31. T. Yu *et al.*, Modulation of M2 macrophage polarization by the crosstalk between Stat6 and Trim24. *Nat. Commun.* **10**, 4353 (2019).
32. S. F. Rocha *et al.*, Esm1 modulates endothelial tip cell behavior and vascular permeability by enhancing VEGF bioavailability. *Circ. Res.* **115**, 581–590 (2014).
33. E. N. Arwert *et al.*, A unidirectional transition from migratory to perivascular macrophage is required for tumor cell intravasation. *Cell Rep.* **23**, 1239–1248 (2018).
34. A. Lapenna, M. De Palma, C. E. Lewis, Perivascular macrophages in health and disease. *Nat. Rev. Immunol.* **18**, 689–702 (2018).
35. M. E. Pitulescu *et al.*, Dll4 and Notch signalling couples sprouting angiogenesis and artery formation. *Nat. Cell Biol.* **19**, 915–927 (2017).
36. M. Fernández-Chacón, I. García-González, S. Mühleder, R. Benedito, Role of Notch in endothelial biology. *Angiogenesis* **24**, 237–250 (2021).
37. V. C. Luca *et al.*, Structural basis for Notch1 engagement of Delta-like 4. *Science.* **347**, 847–853 (2015).
38. A. Matsuura *et al.*, *O*-linked *N*-acetylglucosamine is present on the extracellular domain of notch receptors. *J. Biol. Chem.* **283**, 35486–35495 (2008).
39. M. Z. Mehboob, M. Lang, Structure, function, and pathology of protein O-glucosyltransferases. *Cell Death Dis.* **12**, 71 (2021).
40. F. Bartolo *et al.*, Pro-angiogenic macrophage phenotype to promote myocardial repair. *J. Am. Coll. Cardiol.* **73**, 2990–3002 (2019).
41. P.-Y. Bai *et al.*, Environmental eustress improves postinfarction cardiac repair via enhancing cardiac macrophage survival. *Sci. Adv.* **8**, eabm3436 (2022).
42. C. Mazio *et al.*, Pre-vascularized dermis model for fast and functional anastomosis with host vasculature. *Biomaterials* **192**, 159–170 (2019).
43. A. P. Veith, K. Henderson, A. Spencer, A. D. Sligar, A. B. Baker, Therapeutic strategies for enhancing angiogenesis in wound healing. *Adv. Drug Deliv. Rev.* **146**, 97–125 (2019).
44. K. L. Spiller *et al.*, Sequential delivery of immunomodulatory cytokines to facilitate the M1-to-M2 transition of macrophages and enhance vascularization of bone scaffolds. *Biomaterials* **37**, 194–207 (2015).
45. K. E. Martin, A. J. García, Macrophage phenotypes in tissue repair and the foreign body response: Implications for biomaterial-based regenerative medicine strategies. *Acta Biomater.* **133**, 4–16 (2021).
46. E. Vagesjo *et al.*, Perivascular macrophages regulate blood flow following tissue damage. *Circ. Res.* **128**, 1694–1707 (2021).
47. E. Khmelewski, A. Becker, T. Meinertz, W. D. Ito, Tissue resident cells play a dominant role in arteriogenesis and concomitant macrophage accumulation. *Circ. Res.* **95**, e56–e64 (2004).
48. C. E. Bergmann *et al.*, Arteriogenesis depends on circulating monocytes and macrophage accumulation and is severely depressed in op/op mice. *J. Leukoc. Biol.* **80**, 59–65 (2006).
49. C. Troidl *et al.*, The temporal and spatial distribution of macrophage subpopulations during arteriogenesis. *Curr. Vasc. Pharmacol.* **11**, 5–12 (2013).
50. P. Libby, Inflammation in atherosclerosis. *Nature* **420**, 868–874 (2002).
51. P. Libby, Inflammation in atherosclerosis. *Arterioscler. Thromb. Vasc. Biol.* **32**, 2045–2051 (2012).
52. T. Masuda *et al.*, Specification of CNS macrophage subsets occurs postnatally in defined niches. *Nature* **604**, 740–748 (2022).
53. D. J. Moloney *et al.*, Mammalian Notch1 is modified with two unusual forms of O-linked glycosylation found on epidermal growth factor-like modules. *J. Biol. Chem.* **275**, 9604–9611 (2000).
54. K. T. Schjoldager, Y. Narimatsu, H. J. Joshi, H. Clausen, Global view of human protein glycosylation pathways and functions. *Nat. Rev. Mol. CELL Biol.* **21**, 729–749 (2020).